Journal of the European Ceramic Society 19 (1999) 561–569

PII: S0955-2219(98)00227-1
0955-2219/99/$—see front matter

Microstructural and Mechanical Characterization of SiC-submicron TiB_2 Composites

C. Blanc,† F. Thevenot* and D. Goeuriot

Centre SMS, Ecole Nationale Supérieure des Mines de Saint-Etienne, 42023 Saint-Etienne Cedex 2, France

(Received 6 March 1998; accepted 16 September 1998)

Abstract

The aim of this work is to characterize ceramic composites SiC–TiB_2. After preparation of dense composites αSiC–TiB_2 (5, 10 and 15 vol% TiB_2) by reactive pressureless sintering, the materials have been characterized by their microstructure and their mechanical properties. The dispersion of TiB_2 particles is quite homogeneous, observed both by optical and scanning electron microscopies. Image analysis has revealed a majority of submicronic particles. Atomic force and transmission electron microscopies have shown the presence of nanometric TiB_2 particles. Concerning mechanical properties, toughness increases with the TiB_2 content, whereas hardness decreases when the TiB_2 content increases. © *1999 Elsevier Science Limited. All rights reserved*

Keywords: composites, borides, mechanical properties, SiC, TiB_2.

1 Introduction

Carbide and boride ceramics have attractive intrinsic characteristics, i.e. high melting point, high hardness, good mechanical inertness, high wear resistance and good strength, that makes them suitable candidates for mechanical and tribological applications.

Several authors have already studied composites SiC–TiC and SiC–TiB_2.[1–4] But if they have studied the effect of TiB_2 addition to αSiC on mechanical properties, they haven't studied precisely the microstructure of the composites.

In a previous work, we have described the preparation of composites SiC–TiB_2 (5, 10 and 15 vol% TiB_2) from TiO_2, B_4C and a phenolic resin, used as carbon precursor.[5] The present paper focuses on the microstructural characterization of the materials using optical, scanning electron, atomic force, and transmission electron microscopies. These microstructures are correlated with mechanical properties.

Finally, this paper will use a model to explain the reinforcement of the composite. Wear tests were also performed using a pin on flat configuration; the results will be published in another paper.[22]

2 Experimental Procedures

The starting powders are commercially available:

- αSiC, A10 from STARCK, specific surface SS = 14–17 m^2/g, mean grain size $d_{50} = 0{\cdot}75\ \mu m$, 1·1 wt% oxygen.
- B_4C, HS from STARCK, SS = 15–20 m^2/g, $d_{50} = 1{\cdot}5\ \mu m$, 1·7 wt% oxygen.
- TiO_2 rutile, ALDRICH, with agglomerates 200–300 nm, purity > 99%.

A phenolic resin (PERSTORP, S.A. FRANCE) is used as carbon source.

After milling and dispersion of the powders in water, drying and sieving, pressureless reactive sintering under argon was carried out.

The resin is cured during 2 h at 180°C, then cracked under argon at 850°C during 4 h.

The following reaction takes place at 1400°C:

$$TiO_2 + 0{\cdot}5B_4C + 1{\cdot}5C \rightarrow TiB_2 + 2CO$$

This work is part of the PhD Thesis of C. Blanc, Ecole des Mines, 18 December 1997.

*To whom correspondence should be addressed. Fax: +33 47742 0000; e-mail: thevenot@emse.fr

The complete sintering cycle is the following:

- temperature rise, 10°C min^{-1} up to 1400°C and reaction for the TiB_2 formation, 4 h at 1400°C, under vacuum
- then temperature rise, 10°C min^{-1} up to 2190°C, 1 h dwell, then cooling 15°C min^{-1}, under argon (Table 1).

The samples were characterized by their density, their microstructure and their mechanical properties (Vickers microhardness, fracture toughness based on cracks measurements after Vickers indentations). An industrial αSiC reference material is considered (mean grain size 5 μm) (Table 1).

For the toughness determination we used the relation proposed by Evans and Charles.

$$K_{1c} = 0{\cdot}057H\sqrt{a}\left(\frac{E}{H}\right)^{2/5}\left(\frac{c}{a}\right)$$

H: hardness GPa
a : half Vickers print size μm
c : half crack length μm
E : Young modulus GPa

Concerning the microstructures, diamond polished samples were observed by an optical microscope, then by a SEM, and finally by a AFM which revealed nanometric precipitates. Thin foils were prepared with the composite containing 5 vol% of TiB_2 in order to observe and to characterize the nanometric precipitates by TEM. Thin foils were prepared by standard techniques, i.e grinding, polishing, and dimpling to a thickness close to 30 μm, followed by Ar ion beam thinning.

In order to predict values for the toughness of our composites, we have used the calculation of residual stresses in a matrix containing particles, carried out by Taya *et al.*,[6] using a model proposed by Eshelby[7] and modified for a finite volume fraction of particles.[8–11] This enables the calculation of the decrease of the stress intensity factor ΔK_T due to the compressive residual stress in the matrix, and thus the increase in the crack growth resistance.

3 Results and Discussion

3.1 Properties of materials

The properties of materials (density, hardness and toughness) are given in Table 1. Hardness decreases when the TiB_2 content increases, and toughness seems to increase slightly with the percentage of TiB_2. This will be discussed later on.

3.2 Optical microscopy — image analysis

Of course the resolution of optical microscopy is limited but it allows a good general panorama of the microstructures; other techniques will be used to characterize the finest particles, not detected here: it is interesting to discover the different results obtained by the series of techniques.

Figure 1 shows the microstructures observed by optical microscopy. Every sample presents a homogeneous repartition of white TiB_2 particles. Furthermore, the distance between particles decreases when the TiB_2 content increases.

These optical observations have been confirmed by image analysis. As we have shown earlier,[5] the particles size of TiB_2 increases with the TiB_2 content (Table 1):

- 75% of TiB_2 particles have a grain size less than 1 μm in samples containing 5 vol% TiB_2
- 60% in the case of 10 vol% TiB_2
- 55% in the case of 15 vol% TiB_2.

The inter particles distance r has been determined.

The distribution of radius is given in Fig. 2. The distance r between particles increases when the TiB_2 content drops. The radius corresponding to the highest number of particles varies from 1 μm for 15 vol% TiB_2, to 1·5 μm for 10 vol% TiB_2, and to 2 μm for 5 vol% TiB_2.

Finally, the particles seem to coalesce and coarsen in samples containing 10 and 15 vol% TiB_2: there are more particles, therefore the distance between them decreases, and so the coalescence proceeds during sintering (Fig. 1).

3.3 Scanning electron microscopy

The distribution of TiB_2 particles is again homogeneous (Fig. 3). TiB_2 particles appear in white,

Table 1. Properties of materials

Materials	*Sintering temperature*	*% Density*	*% of TiB_2 (1) particles < 1 μm*	*Hardness (2) (GPa)*	*Toughness (3) $MPa\sqrt{m}$*
SiC industrial reference	—	97	—	22 ± 1	$3{\cdot}1_8 \pm 0{\cdot}3$
SiC—5 vol % TiB_2	2190°C 1 h	98	75	30 ± 1	$3{\cdot}5_8 \pm 0{\cdot}4$
SiC—10 vol % TiB_2	2190°C 1 h	97	60	27 ± 1	$3.6_5 \pm 0{\cdot}4$
SiC—15 vol% TiB_2	2190°C 1 h	95	55	23 ± 2	$3{\cdot}9_5 \pm 0{\cdot}4$

(1) Image analysis method;(2) Vickers microhardness (5 N, 30 s);(3) Vickers indentation fracture method (10 N, 30 s).

SiC is grey. Black particles (arrows) may be observed, they are in contact with some TiB_2 particles.

The chemical analysis of the later black particles by microanalysis (EDS, WDS) was not possible, due to their low size ; the analysis includes also SiC matrix and TiB_2 particles. It may be assumed that they correspond to an excess of B_4C or carbon, not reacted with TiO_2 during synthesis (cf. § 2). This hypothesis will be confirmed later by TEM.

Chemical etching with MURAKAMI solution has been used (Fig. 4). This solution reveals the

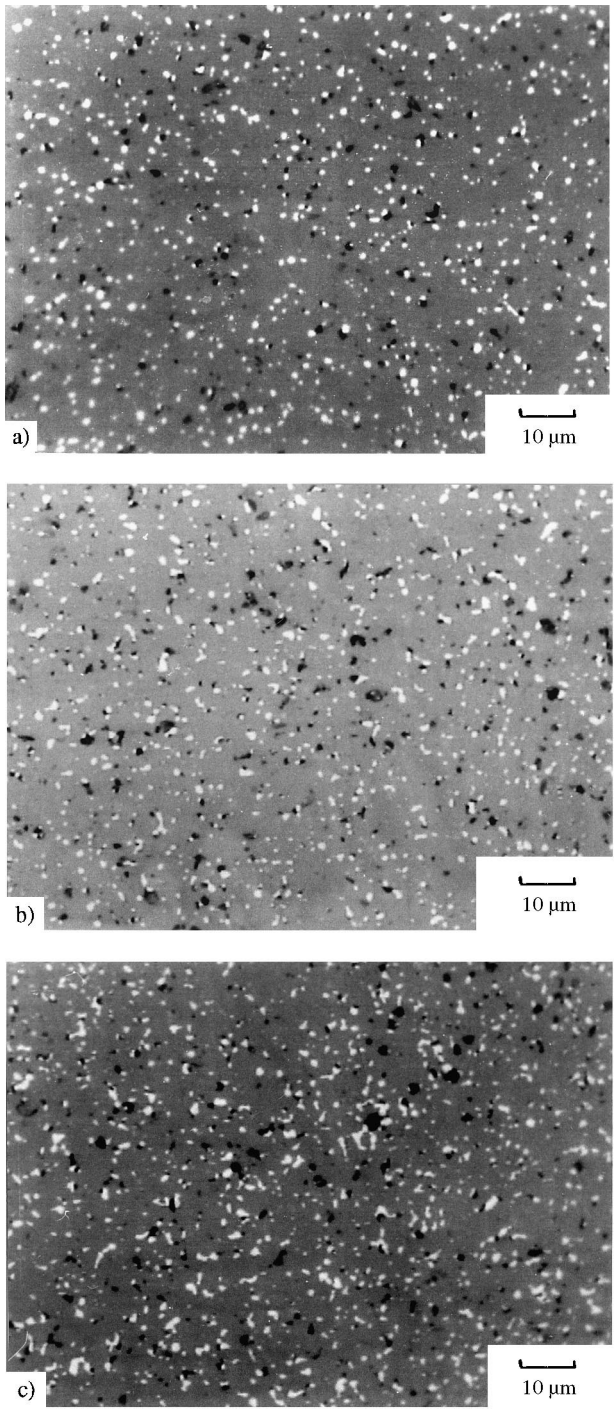

Fig. 1. Optical microstructure of composites: (a) SiC/5 vol% TiB_2 (SiC matrix in gray, TiB_2 in white); (b) SiC/10 vol% TiB_2; (c) SiC/15 vol% TiB_2.

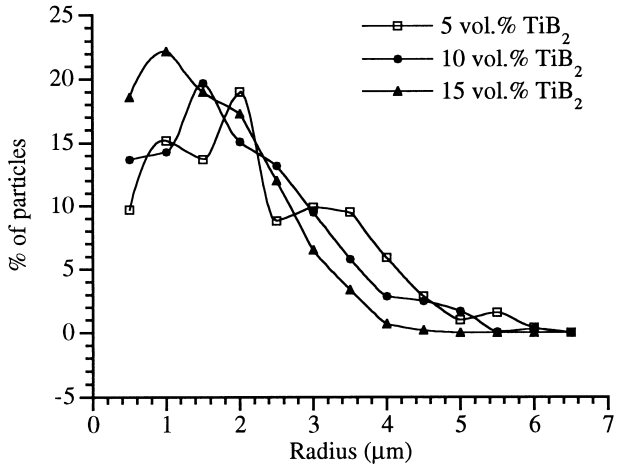

Fig. 2. Distribution of distance between particles of TiB_2.

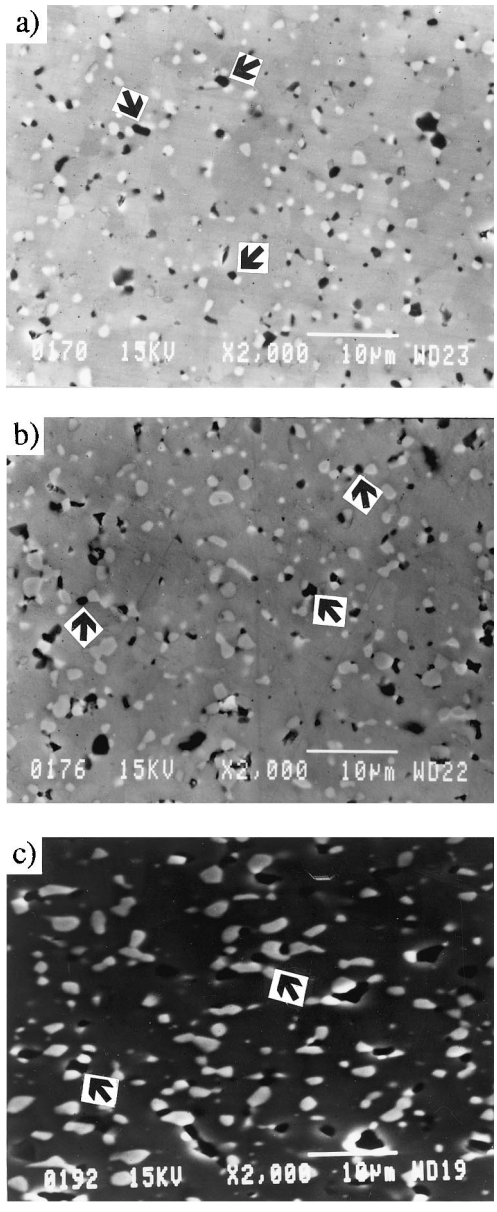

Fig. 3. SEM microstructures of composites before chemical attack (SiC matric in gray, TiB_2 in white, 'dark particles' are arrowed): (a) SiC/5 vol% TiB_2; (b) SiC/10 vol% TiB_2; (c) SiC/15 vol% TiB_2.

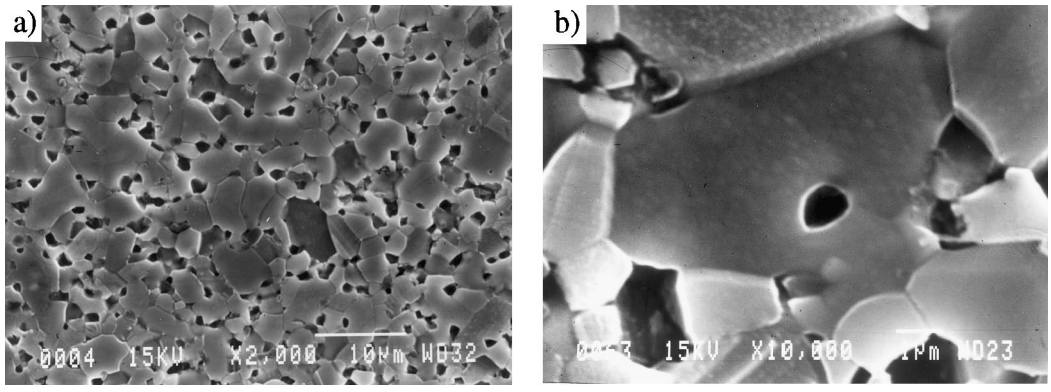

Fig. 4. SEM microstructures of composites after chemical etching: (a) microstructure of the SiC matrix (TiB_2 has disappeared during etching); (b) intragranular porosity.

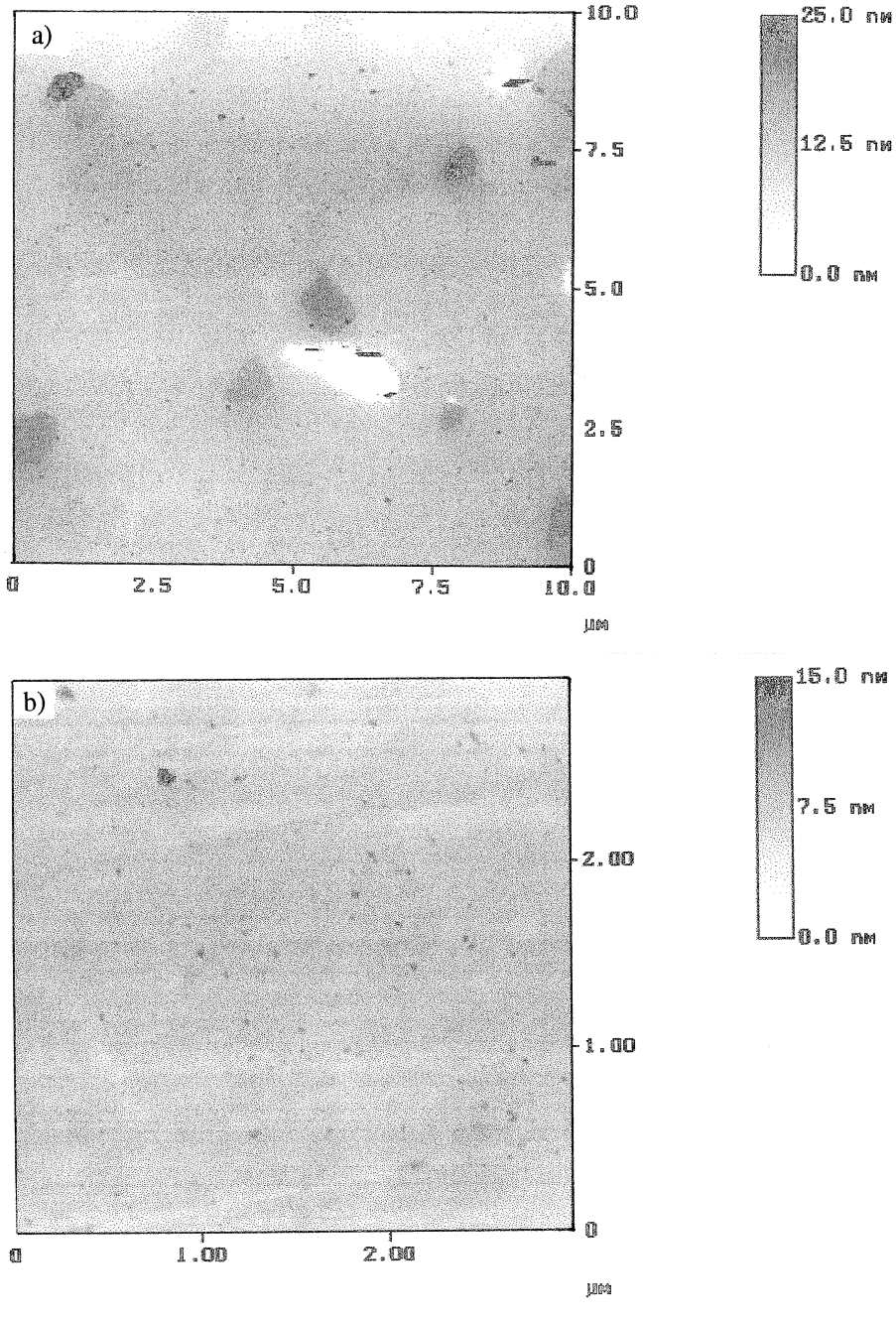

Fig. 5. (a) Topographic image obtained by AFM of SiC/5 vol% TiB_2; (b) Detail of a. Finer population of particles can be observed.

microstructure of SiC, but TiB_2 particles are dissolved and disappear. Equiaxed 3–8 μm SiC grains are observed (mean grain size 4 μm); this size does not depend on the TiB_2 content [Fig. 4(a)]. Porosities come from initial material porosity, and from the dissolution of TiB_2 and black particles during etching. Some porosities are intragranular after etching [Fig. 4(b)], that seems to indicate that some TiB_2 particles and/or some porosities were intragranular after sintering; this assumption will be confirmed by TEM.

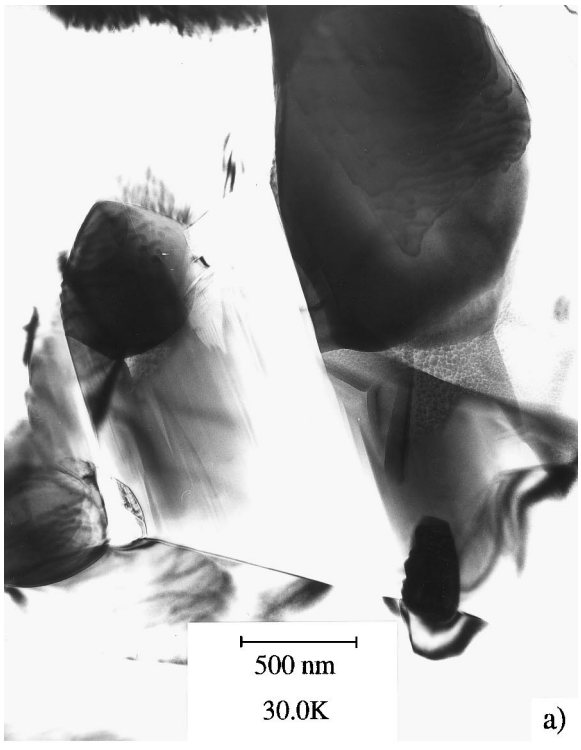

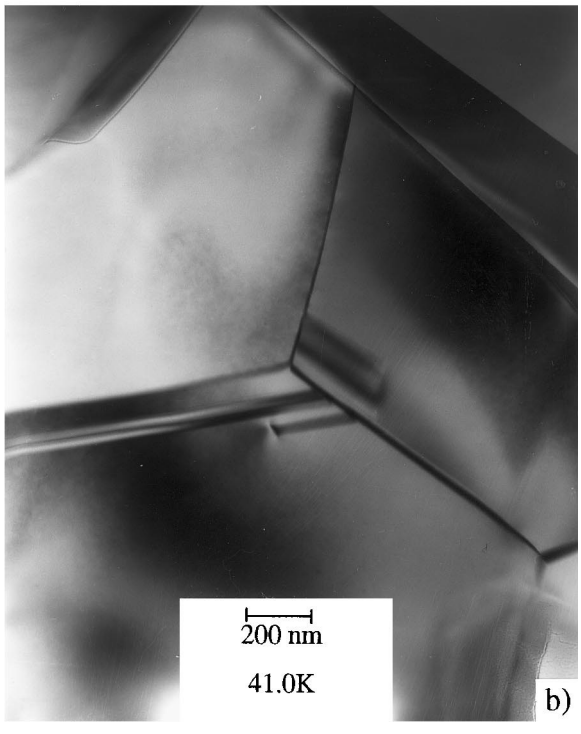

Fig. 6. (a) General view of the SiC/5 vol% TiB_2 composite (bright field image); (b) grain boundaries of SiC (bright field image).

3.4 Atomic force microscopy (AFM)

AFM allows to obtain the topography of materials surface, measuring the flexion of a lever when the micro tip fixed at its end explores the sample surface. A 5 vol% TiB_2 composite was examined.

The width of the observed zone is a 10 μm side square. This technique evidences two particles populations, in relief over the sample surface (Fig. 5):

1. the size of larger particles is 900 nm × 600 nm. They constitute a flat plateau and a relief of 7 nm over the matrix plan ($\Delta Z = 7$ nm)
2. much smaller particles, non visible using optical microscopy or even SEM; the larger have a size range of 60 to 120 nm and ΔZ of 5 to 12 nm. The finer have a size close to 40 nm and $\Delta Z = 2$ nm.

For the first time, AFM allowed to reveal the existence of nanometric particles. But there is no information about the nature of these nanometric precipitates. The materials have been then observed by TEM, in order to identify the nature of these particles.

3.5 Transmission electron microscopy (TEM)

Figure 6(a) gives a general view of the 5 vol% TiB_2 material: we can observe SiC grains (3–6 μm) and particles in intergranular position.

Grain boundaries between SiC grains seem to be 'clean'; with a magnification of 200 000, no glassy phase at triple joint junctions can be observed [Fig. 6(b)].

Small grains, in intergranular sites, have a size in the 0·5–1·5 μm range. There are three kinds of grains: TiB_2, B_4C and graphite (determined by diffraction).

In Fig. 7, three neighbour grains are observed: they are respectively, a TiB_2 grain (top), graphite (in the center) and a B_4C grain. This observation

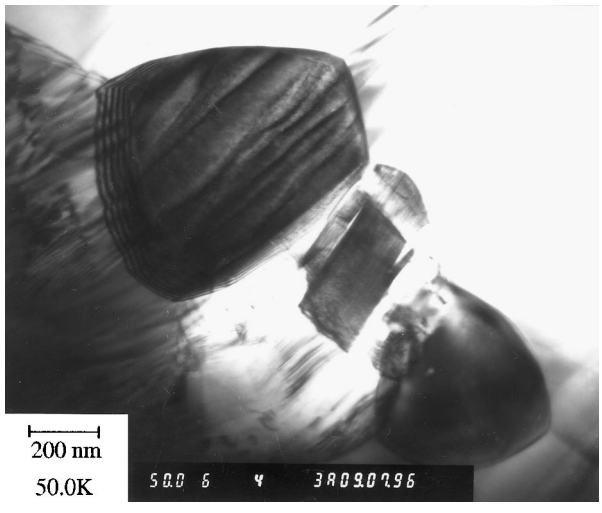

Fig. 7. Bright field image of three particles: respectively TiB_2, graphite and B_4C.

proves that starting reactive products leading to TiB_2, are still remaining. We can now answer the question in § 3·3: black grains observed by SEM are constituted by B_4C or graphite (Fig. 3).

TiB_2 precipitates are present in two positions:

- if they are intergranular, they are elongated, with a size of at least 0·2 μm [Fig. 8(a)]; they are identified to hexagonal TiB_2 by diffraction [Fig. 8(b)]
- if they are intragranular, they are round, with a size of 60–200 nm [Fig. 9(a)]. Some of them are surrounded by dislocations [Fig. 9(b)]; these dislocations may be due to residual stresses around the precipitates. In the matrix, several precipitates of the same kind may be sometimes observed in a single SiC grain [Fig. 9(c)].

All the TiB_2 precipitates are produced according to the chemical reaction, occurring at 1400°C and mentioned in § 2. Precipitates with different sizes are produced; then during the sintering of the composite, SiC grains grow and include or trap the smallest precipitates. The other larger TiB_2 precipitates, hinder grain coarsening, and remain in intergranular positions. An estimate of the intra/intergranular limit for the TiB_2 position, may be close to 200 nm.

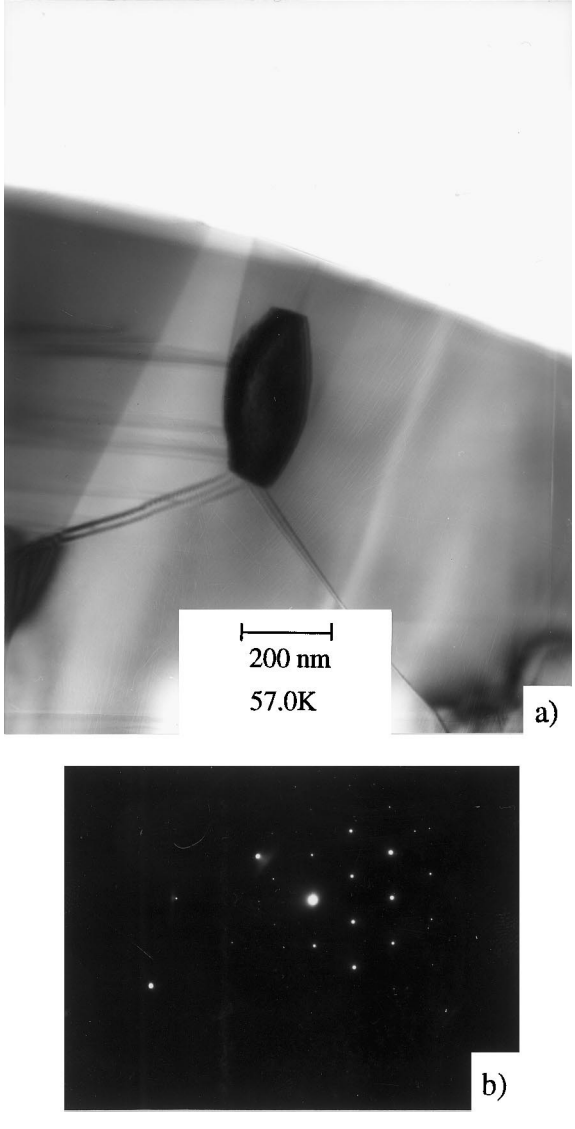

Fig. 8. (a) Bright field image of a TiB_2 intergranular particle; (b) Diffraction of this particle. Zone axe [001], the hexagonal structure of the base plane of TiB_2 can be seen.

At this point, we have stated a convenient and complete description of the microstructure of our composites. Considering (i) the preparation route using reactive sintering, in conditions close to industrial ones, using water slurries for instance, is original and the materials obtained too, and (ii) the toughening of usual micronic SiC–TiB_2 has been already widely observed in the literature,[4,12–17] we estimate it is legitimate to determine the toughness of our materials and to compare it with an analytical model proposed by Taya *et al.*[6]

3.6 Mechanical characterization

An industrial αSiC material, using the same A10 starting powder, manufactured in similar conditions, with a mean grain size close to 5 μm, has been considered, as an element for comparisons (Table 1).

The results are presented in Table 1.

Even though the hardness decreases when the TiB_2 content increases, the composites present a higher hardness than the single phase SiC. Thus TiB_2 is harder than SiC, a higher hardness should be obtained when the TiB_2 content increases. In our case, the porosity influence is predominant: the hardness drops when the porosity increases with the increasing TiB_2 percentage.

Toughness of composites is slightly higher than a single phase SiC.

We have calculated the residual stresses in the materials, using an analytical model.[6]

The first step consists of the calculation of average residual stresses of thermal origin in the matrix and in the dispersed phase, using the ESHELBY model. In the second step, the stress intensity factor change ΔK_T, due to residual compressive stresses in the matrix, is calculated.

The hypotheses of the model are the following; the composite consists of three phases:

- spherical particulates of volume fraction f_p
- spherical voids of volume fraction f_v (here determined by image analysis).
- and the matrix with its volume fraction $1-f_p-f_v$

In order to calculate the thermal residual stress at room temperature T_R, the composite is assumed to be subjected to a temperature change $\Delta T = T_R - T_P$ (T_P is the creep temperature of the material, here close to 1200°C).

$$\alpha^* = \int_{T_p}^{T_R} \left(\alpha_p(T) - \alpha_m(T)\right) dT$$

where $\alpha_p(T)$: thermal expansion coefficient of particulates $\alpha_m(T)$: thermal expansion coefficient of the matrix.

Taya proposed to use T_p, the processing (sintering) temperature (here 2463 K). But this value leads to excessive irrealistic values of tensile stress on TiB_2 particles (here $\sigma_p = 2600$–3000 MPa). Therefore, we assumed that the material goes from a creep state, to a purely elastic state at $T_p = 1473$ K, value which has been used in our calculations.

Also, the thermal residual stresses in the composite are assumed to be induced by elastic deformations of the matrix and particulates under a uniform temperature variation ΔT.

In a first step, we calculate the α^* deformation, induced by the thermal expansion coefficient mismatch between the matrix and the particulates: $\alpha^* = -3{\cdot}6 \times 10^{-3}$.

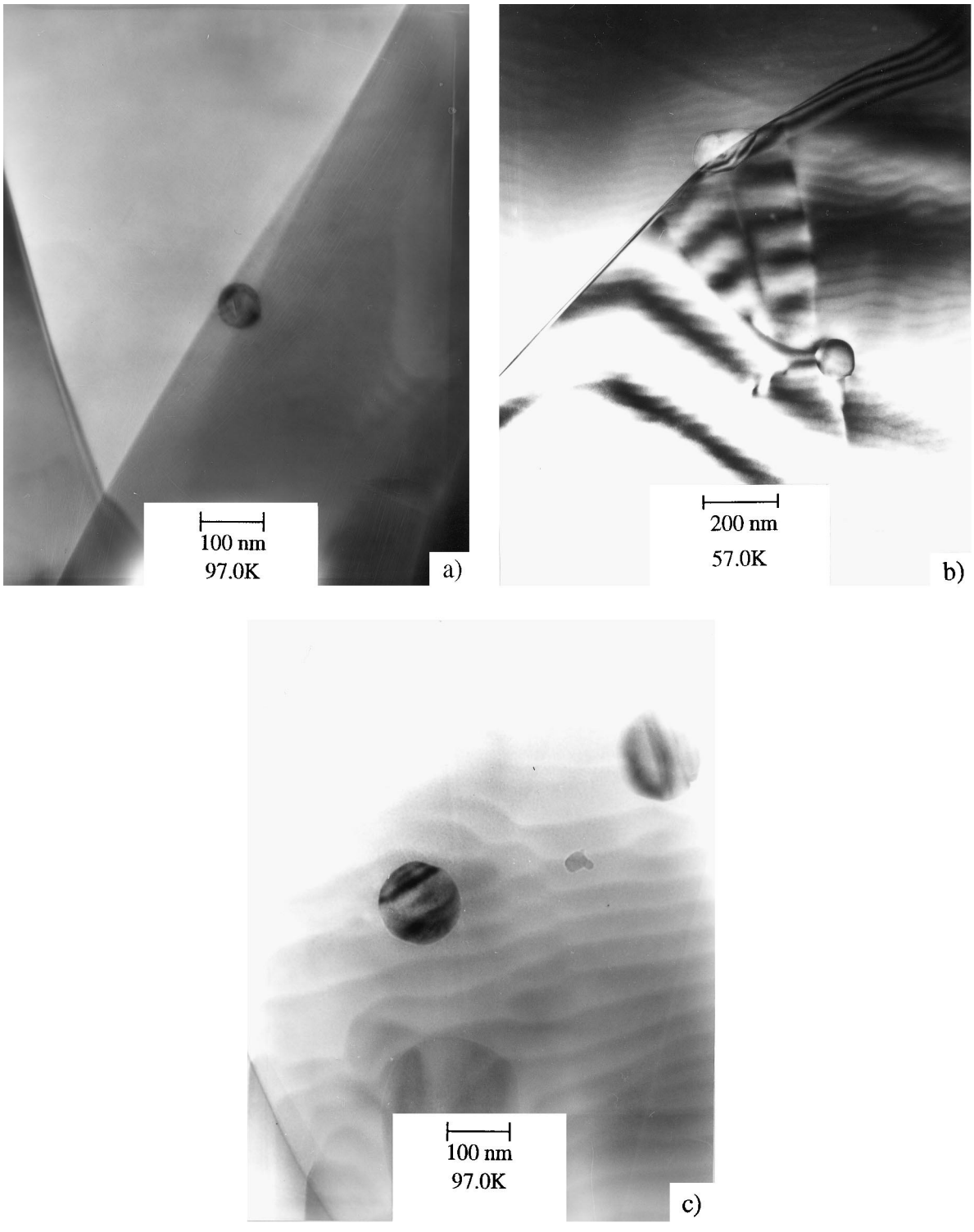

Fig. 9. Bright field image TEM: (a) TiB_2 precipitate (60 nm); (b) TiB_2 precipitate with dislocations; (c) two TiB_2 precipitates in a same SiC grain.

Table 2. Residual stresses on TiB_2 (σ_p) and SiC (σ_m) particles, stress intensity factor reduction or increase of theoretical toughness ΔK_T, experimental increase ΔK_E, in the composites materials

Materials	*Volume fraction of particles* f_p	*Volume fraction of voids* f_v	*Tensile stress* σ_p *MPa*	*Compressive stress* σ_m *MPa*	d μm	λ μm	ΔK_T $MPa\sqrt{m}$	ΔK_E $MPa\sqrt{m}$
SiC–5 vol% TiB_2	0.05	0·025	1475	−80	0·6	2·2	+0·16	0·4
SiC–10 vol% TiB_2	0·10	0·032	1375	−160	0·8	2	+0·28	0·47
SiC–15 vol% TiB_2	0·15	0·053	1270	−240	0·9	1·6	+0·32	0·77

The average residual stresses, of thermal origin, may be calculated, for the particle (σ_p) and matrix (σ_m), knowing f_p, f_v and constants (Young's modulus, Poisson's ratio) of SiC and TiB_2 (Table 2).

In a second step, we calculate the stress intensity factor reduction ΔK_T due to thermal residual stress in the matrix:

$$\Delta K_T = 2q \times \sqrt{\frac{2(\lambda - d)}{\pi}}$$

where

λ = interparticulates TiB_2 spacing (determined by image analysis)
d = average diameter of TiB_2 particles (image analysis)
q = local average compressive stress (here $\langle\sigma\rangle_m$)

This reduction in ΔK_T is equivalent to the increase in the crack growth resistance by the same amount. This allows to compare the increase of theoretical toughness ΔK_T obtained by this model, with the experimental one ΔK_E (Table 2)

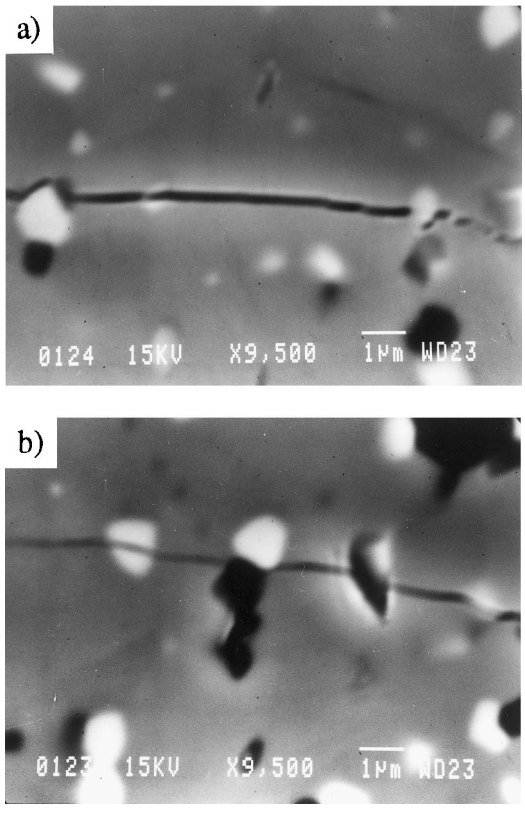

Fig. 10. SEM observations of typical cracks paths induced by Vickers indentation: (a) crack deflection around TiB_2 particles; (b) TiB_2 particle sheared by a crack.

$$\Delta K_E = (K_{1C})\text{composite} - (K_{1C})\text{monolithic}$$

The difference between experimental and analytical results allows to explain partially the reinforcement of the material by TiB_2 particulates.

In fact, residual stresses of thermal origin may induce a crack deflection phenomenon.

We found that the SiC matrix is under compression, while TiB_2 particles are in tension when $\alpha_p > \alpha_m$: the particulate tends to contract more than the matrix during cooling, that submits the particulate to tension while inducing circonferential compressive stresses within the matrix.[18] This improves the mechanical properties at room temperature, because the crack turns round the particle.

Therefore, the mismatch between thermal expansion coefficients α_m and α_p, creates stress fields around the dispersoids during the elaboration process. These stresses are revealed by TEM by the presence of dislocations around TiB_2 particles [Fig. 9(b)]. A crack tends to propagate parallel to the direction of local compressive forces and perpendicular to the direction of local tension stresses.[18]

The energy needed by the crack propagation is increased by this path changing: it is the crack deflection.

Here, the SEM observation of cracks induced by Vickers indentations has shown the crack deflection around the TiB_2 particles [Fig. 10(a)]. Meanwhile, sometimes cracks cross over and shear the particle [Fig. 10(b)].

But all these facts are not sufficient to explain completely the observed reinforcement:

1. if the tensile stresses are high enough, microcracking in the matrix may take place. This microcracking induces the division of large cracks into several smaller cracks, thus dissipating energy by creating new free surfaces. The model of Taya *et al.*[6] leads to high values of tensile stresses, close to twice the value of rupture strength of the matrix (even with the choice of an optimum value for T_p). In spite of these high values, no cracks are observed by SEM.

   Two hypotheses can be proposed:

   - the microcracks are formed but are too small to be revealed.

- the microcracks are not formed because the critical diameter R_c of particles (4–5 μm), among which cracks are provoked, is not reached (mean grain size of TiB_2 less than 1 μm in our case).

2. A discontinuity in the bulk (porosity, particle detached from the matrix) may stop the crack. Several authors have discussed the toughening by TiB_2 particulates. According to them reinforcement may be due to microcracking, crack deflection and crack bridging by the particles[15,19] or only by bridging.[20] The difference between the coefficients of thermal expansion of TiB_2 and SiC induces microstresses leading to crack deflection at the SiC/TiB_2 weak interface.[12,21]

In conclusion, toughness may increase slightly with the TiB_2 content. SEM observations and analytical calculation tend to identify the well known deflection of the crack by the particles. But this hypothesis is not sufficient to explain the reinforcement completely. Other hypotheses, like microcracking, even not experimentally observed, might be evoked.

4 Conclusions

Considering the microstructure, all the materials have a homogeneous TiB_2 particulates repartition. The mean grain size of TiB_2 increases with its content: 75% are less than 1 μm for 5 vol%, 60% for 10 vol%, and 55% for the 15 vol% TiB_2 composite.

Furthermore, AFM indicates the presence of nanometric particles (100–200 nm), not visible with optical microscopy and SEM. TEM allows their observation and their identification (TiB_2, B_4C, C).

One main interest of this work is to show that reactive pressureless sintering leads to a very fine grain composite, that is not possible starting from mixtures of TiB_2 and SiC powders and simple sintering (with/without pressure). Finally, mechanical properties (hardness, toughness) have been measured. Different mechanisms (crack deflection by TiB_2 particles, microcracking...) may be involved to explain a slight reinforcement.

References

1. Endo, H., Ueki, M. and Kubo, H., Hot pressing of SiC–TiC composites. *J. Mat. Sci.*, 1990, **25**, 2503–2506.
2. Ohya, Y., Hoffmann, M. J. and Petzow, G., Mechanical properties of hot pressed SiC–TiB_2/TiC composites synthesized in situ. *J. Mater. Sci. Letters*, 1993, **12**, 149–152.
3. Yoon, J. D. and Kang, S. G., Strengthening and toughening behavior of SiC with additions of TiB_2. *J. Mater. Sci. Letters*, 1995, **14**, 1065–1067.
4. McMurty, C. H., Boecker, W. D. G., Seshadri, S. G., Zanghi, J. S. and Garnier, J. E., Microstructure and materials properties of SiC–TiB_2 particulate composites. *Am. Ceram. Soc. Bull.*, 1987, **66**(2), 325–329.
5. Blanc, C. and Thévenot, F., Processing of ultra-fine dispersion of TiB_2 in SiC ceramic matrix. *Mater. Sci. Forum*, 1997, **235–238**, 249–254.
6. Taya, M., Hayashi, S., Kobayashi, A. S. and Yoon, H. S., Toughening of a particulate reinforced ceramic–matrix composite by thermal residual stress. *J. Am. Ceram. Soc.*, 1990, **73**(5), 1382–1391.
7. Eshelby, J. D., The determination of elastic fields of an ellipsoidal inclusion and related problems. *Proc. R. Soc. London.*, 1957, **A241**, 376–396.
8. Mori, T. and Tanaka, K., Average stress in matrix and average energy of materials with misfitting inclusions. *Acta Metall.*, 1973, **21**, 571–574..
9. Mura, T., *Micromechanics of Defects in Solids*, 2nd edn. Ch. 7 Martinus Nijhoff, The Hague, The Netherlands, 1987.
10. Taya, M. and Arsenault, R. J., *Metal Matrix Composites: Thermomechanical Behavior*, Ch. 3. Pergamon Press, Oxford, UK. 1989.
11. Takao, Y. and Taya, M., Thermal expansion coefficients and thermal stresses in an aligned short fiber composite with application to a short carbon fiber/aluminum. *J. Appl. Mech.*, 1985, **52**, 806–810..
12. Ohya, Y., Hoffmann, M. J. and Petzow, G., Sintering of in-situ synthesized SiC–TiB_2 composites with improved fracture toughness. *J. Am. Ceram. Soc.*, 1992, **75**(2), 2479–2783.
13. Yoon, J. D. and Kang, S. G., Strengthening and toughening behavior of SiC with additions of TiB_2. *J. Mat. Science Letters*, 1995, **14**, 1065–1067.
14. de Mestral, F. and Thévenot, F., Boride-carbide composites: TiB_2–TiC–SiC. In *The Physics and Chemistry of Carbides; Nitrides and Borides*, ed. R. Freer. Kluwer Acad. Publ., Netherlands, 1990, pp. 457–481.
15. Faber, K. T., Gu, W. H., Gani, H. and Winholtz, R. A., Fracture properties of SiC based particulate composites. In *Toughening Mechanism in Quasi-Brittle Materials* ed. S. P. Shah Kluwer Academic Publishers, Dordrecht, The Netherlands, 1991, pp. 3–17.
16. De Mestral, F. and Thévenot, F., Ceramic composites: TiB_2–TiC–SiC. Part I: Properties and microstructures in the ternary system. *J. Mat. Sci.*, 1991, **26**, 5547–5560.
17. De Mestral, F. and Thévenot, F., Ceramic composites: TiB_2–TiC–SiC. Part II: Optimization of the composite 20% TiB_2–55 (mol%) TiC–25% SiC. *J. Mat. Sci.*, 1991, **26**, 5561–5565.
18. Wei, G. C. and Becher, P. F., Improvements in mechanical properties in SiC by the addition of TiC particules. *J. Am. Ceram. Soc.,* 1984, 571–574.
19. Cai, H., Gu, W. H. and Faber, K. T., Microcrack toughening in a SiC–TiB_2 composite. In *Proceedings of the American Society for Composites, Fifth Technical Conference on Materials*. Technomic Publishing Company, Lancaster, PA, 1990, pp. 892–901.
20. Kuo, D. H. and Kriven, W. M., Mechanical behavior and microstructure of SiC and SiC/TiB_2 ceramics. *J. Eur. Ceram. Soc.*, 1998, **18**, 51–57.
21. Zhang, G. J., Yue, X. M., Jin, Z. Z. and Dai, J. U., In situ synthesized TiB_2 toughened SiC. *J. Eur. Ceram. Soc.*, 1996, **16**, 409–412.
22. Blanc, C., Thevenot, F. and Treheux, D., Wear resistance of αSiC-TiB_2 composites prepared by reactive sintering. *J. Eur. Ceram. Soc.*, 1999, **19**(5), 571–579.